Desalination and Water Treatment
www.deswater.com
doi: 10.1080/19443994.2015.1110717

57 (2016) 20817–20836
September

Taylor & Francis
Taylor & Francis Group

Removal of cadmium and zinc ions from industrial wastewater using nanocomposites of PANI/ZnO and PANI/CoHCF: a comparative study

Mohammad Ali Moosavian, Nima Moazezi*

Faculty of Engineering, Department of Chemical Engineering, University of Tehran, P.O. Box 11365-4563, Tehran, Iran, emails: moosavian@ut.ac.ir (M.A. Moosavian), nmoazezi@ut.ac.ir (N. Moazezi)

Received 29 December 2014; Accepted 13 October 2015

ABSTRACT

Polyaniline (PANI) adsorbents functionalized with zinc oxide nanoparticles (ZnO-NPs) and cobalt hexacyanoferrate (CoHCF) were prepared by chemical precipitation method and they were applied in order to adsorb Cd(II) and Zn(II) from industrial wastewater. First, the adsorbents were characterized by FTIR and XRD analyses for comparison. The adsorption capacity of the polyaniline/CoHCF nanocomposite (PANI/CoHCF/NC) were greater than that of polyaniline/ZnO nanocomposite (PANI/ZnO/NC). PANI/CoHCF/NC was characterized by FTIR, XRD, TEM, SEM, and BET analyses. Experimental parameters affecting Cd (II) and Zn(II) sorption onto the PANI/CoHCF/NC such as pH, adsorbent dosage, contact time, initial concentration of metal ions, and temperature were studied. The kinetic data were analyzed by the pseudo-first-order and pseudo-second-order kinetic models. Consequently, the pseudo-second-order model best described the adsorption of Cd(II) and Zn(II) ions. The equilibrium data was fitted to three isotherm models: Freundlich, Langmuir, and Dubinin–Radushkevich (D–R), and it was shown that the Langmuir model gave the best fit to the experimental data. Thermodynamic parameters showed that the adsorption of these ions onto the PANI/CoHCF/NC was endothermic and spontaneous. The mechanism of sorption was also discussed.

Keywords: Nanocomposite; Adsorption; Polyaniline; Zinc; Cadmium

1. Introduction

Due to their special properties, solid materials with nanometer dimensions have attracted the attention of many researchers around the world [1]. Nanoscaled materials compared with the bulk mode have different chemical and physical behaviors because they have higher number of atoms on the surface [2]; as a result, using these materials leads to changes in coordination number, orbital symmetry, and chemical environment of the elements [3].

Current nanotechnological applications are being reported in oil and related industries [4], health and medicine [5], civil and construction [6], energy [7], automotive and transportation [8], agriculture and food [9], etc.

Other applications of nanoparticles are in water treatment and environmental protection. Recently, application of nanoparticles for the removal of pollutants has become an interesting area of research [10]. Water pollutants, such as aromatic substances [11] and

*Corresponding author.

heavy metals [12] include biological and chemical contaminants [13] seep into underground water, lakes, and rivers [14]. Unlike aromatic substances, heavy metal contaminants are non-biodegradable persisting in the environment [15]. They can seep into water and soil and then it can be adsorbed by plants. As a result, by entering food chain of human beings, they can be dangerously hazardous [16]. In some cases, genetic problems and changes in DNA structure have been observed [17]. The safety limits are specified for each of the heavy metals.

Cadmium (Cd) and Zinc (Zn) are examples of such "heavy metals" which are commonly found in water and wastewater.

Cadmium compounds are used in glass manufacturing, electroplating [18], smelting [19], pigments, plastic [20], and mining [21]. They are commonly found in water and wastewater. Exposure to Cd^{2+} may cause a wide range of adverse health effects for both adults and children. Generally, zinc discharged to the environment from various industrial activities such as mining processing [22] and manufacturing [23] may lead to many diseases which include Itai–Itai disease, carcinogenic [24], renal disturbances, lung insufficiency, bone lesions, cancers [25], and hypertension [26].

So removal of Cd^{2+} and Zn^{2+} from water is an open research area in the global context. Various treatment techniques are available for the removal of Cd^{2+} and Zn^{2+} which include reverse osmosis, solvent extraction, ultrafiltration, phytoremediation, chemical precipitation, adsorption [27].

The major disadvantage of reverse osmosis is the high power consumption due to pumping pressures and the restoration of the membranes [28]. Excessive amount of time and energy for pretreatment limits the application of solvent extraction [29]. The phytoremediation technique has also some limitations such as long contact time required for clean-up and the risk of food chain contamination because of mismanagement and lack of proper care [30]. The chemical precipitation process, which uses large amount of reagents, suffers from sludge production [31]. But the adsorption process is arguably one of the most popular methods for the removal of Cd^{2+} and Zn^{2+} because of its simplicity, convenience, and high removal efficiency [32]. Adsorption is now recognized as an effective and economical method for heavy metal wastewater treatment. The adsorption process offers flexibility in design, operation, and in many cases will produce high-quality, treated effluent. In addition, because adsorption is sometimes reversible, adsorbents can be regenerated by suitable desorption processes [28]. Nanoparticles exhibit good adsorption efficiency especially due to higher surface area and greater active sites for interaction with metallic species. Furthermore, adsorbents with specific functional groups have been developed to improve the adsorption capacity [33].

Efforts to find alternative low-cost materials and the recent progress of nanotechniques have led to the development of new classes of nanoparticles for the treatment of contaminated water [34].

The Prussian blue analogs of chemical formula $\boldsymbol{C}_K\boldsymbol{M}_3[\mathbf{M}(CN)_6]_2{\cdot}nH_2O$ ($\boldsymbol{M}$ = $\mathbf{M}$ = transition metals and $\boldsymbol{C}$ = alkali ion) are constructed from octahedral $\mathbf{M}(CN)_6^{3-}$ complexes, which are bridged into a simple cubic lattice by M^{2+} ions [35]. Nowadays, growing attention is being paid to Prussian blue analogs for their applications in optical and electrochemical properties [36], sensor and biosensor [37], CO_2 and SO_2 capture and separation applications [38], etc. Prussian blue analogs nanomaterials often exhibit excellent size and shape, dependent chemical and physical properties, which cannot be observed in their bulk analogs [39]. So, there is a strong desire to prepare the Prussian blue analogs with nanoscale sizes and shapes in order to investigate their properties. Among the Prussian blue analogs, cobalt hexacyanoferrate (CoHCF) would be especially attractive because of its excellent properties in capacity to store counter cations and ion-exchange selectivity. Moreover, $Co_3[Fe(CN)_6]_2{\cdot}nH_2O$ is a typical Prussian blue analog with different sizes that have been reported at the nanoscale [40].

An environment-friendly material such as ZnO can be used in catalyst industries [41], gas sensors [42], solar cells [43], and UV-absorbers [44]. Recently, scientists have found that nanostructured ZnO could efficiently remove heavy metals [45]. These heavy metals are Cu^{2+} [46], Cd^{2+}, Pb^{2+} [47], and so on.

The development of nano-inorganic/polymer composite material has been receiving significant interest due to wide range of industrial and medical applications [48], photovoltaic applications [49], and ion exchange [31]. These have shown a synergetic behavior between the polymer and inorganic material. Toxic metal ion removal by chelating polymers would be of great importance in environmental application because of reusability, easy handling and having higher adsorption capacities, efficiencies as well as high selectivity to some metal ions [50].

Polyaniline (PANI) has also demonstrated strong adsorption capability to remove heavy metals from water and wastewaters. The existence of positively charged nitrogen atoms in PANI provides a good prospect for their applications in adsorption processes [51].

In this study, PANI adsorbent was prepared by chemical polymerization method for the adsorption of

Cd^{2+} and Zn^{2+} ions from the aqueous solutions. Furthermore, ZnO and CoHCF were added to the PANI for the modification of the adsorbent surface. Between PANI/CoHCF/NC and PANI/ZnO/NC, the best adsorbent is selected for adsorption of metal ions from aqueous solutions for further experiments. Also the effects of selected adsorbent contents, pH, contact time, initial concentration of metal ions, and temperature of the adsorption process were investigated.

2. Experimental

2.1. Chemicals

All chemicals and reagents were of the analytical grade. Potassium hydroxide (KOH), cobalt(II) chloride hexahydrate ($CoCl_2{\cdot}6H_2O$), ZnO, cadmium(II) nitrate nonahydrate ($Cd(NO_3)_2{\cdot}9H_2O$), ammonium peroxydisulfate ($(NH_4)_2S_2O_8$), $ZnCl_2$, potassium ferricyanide ($K_3[Fe(CN)_6]$), hydrochloric acid (37%) (HCl), Nitric acid (65%) (HNO_3), and aniline (C_6H_7N) were obtained from Merck (Germany). Deionized water in this work was obtained from our chemistry laboratory (University of Tehran).

2.2. Preparation of adsorbents

2.2.1. Synthesis of PANI

Chemical polymerization of PANI took place in an aqueous acid solution. Ammonium peroxydisulfate was dissolved in aqueous solution containing hydrochloric acid at 25˚C. Ammonium peroxydisulfate (1 g) was dissolved in 0.1 l of 1 M HCl. The mixture was stirred for 30 min at 25˚C. One milliliter double-distilled aniline was slowly added into the above solution dropwise, under a continuous stirring by Eppendorf Reference 2. After 5 min, a dark green color appeared and then the system was vigorously stirred. After 5 h, the solution was filtered and the precipitate was washed with distilled water. The resulting polymer salt was finally dried at room temperature.

2.2.2. Synthesis of PANI/CoHCF/NC

PANI/CoHCF/NC was synthesized by one-step co-precipitation method. Briefly, 0.237 g of $CoCl_2{\cdot}6H_2O$ (0.01 M of Co^{2+}), 0.329 gr of $K_3[Fe(CN)_6]$ (0.01 M of $K_3[Fe(CN)_6]$) and 1 g Ammonium peroxydisulfate were dissolved in 100 mL of 1 M HCl. The mixture was stirred for 30 min at 25˚C. One milliliter double-distilled aniline was slowly added into the above solution dropwise, under a continuous stirring by Eppendorf Reference 2. After 5 min, a dark green color appeared and then the system was vigorously stirred for 5 h. The solution was filtered and the precipitate was washed with distilled water. The resulting polymer salt was finally dried at room temperature.

2.2.3. Synthesis of PANI/ZnO/NC

PANI/ZnO/NC was synthesized one-step co-precipitation method. Briefly, 0.2 g of ZnO and1 g Ammonium peroxydisulfate were dissolved in 100 mL of 1 M HCl. The mixture was stirred for 0.5 h at 25˚C. One milliliter double-distilled aniline was slowly added into the above solution dropwise, under a continuous stirring by Eppendorf Reference 2. After 5 min, a dark green color appeared and then the system was vigorously stirred for 5 h. The solution was filtered and the precipitate was washed with distilled water. The resulting polymer salt was finally dried at room temperature.

2.3. Instrumentation

Transmission electron microscope (TEM) images were recorded on film on a Philips CM30 TEM operating at 300 kV. TEM was used to determine the size and morphology of PANI/CoHCF/NC. Morphological studies of bare PANI and PANI/CoHCF/NC were carried out by a scanning electron microscope (SEM) S4160 Hitachi model (Tokyo, Japan). The functional groups of bare PANI, PANI/ZnO/NC, and PANI/CoHCF/NC were determined by XRD and FTIR. X-ray powder diffraction (XRD) spectra were taken on a STOE type STIDY-MP-Germany X-ray diffractometer with Copper K-alpha (Cu Kα) radiation. Fourier transform infrared spectrometer (FTIR) measurements were performed using a Bruker Vector 22 FTIR spectrometer with KBr as background within the range of 400–4,000 cm^{-1}. The specific surface area and pore volume were estimated using Brunauer–Emmett–Teller (BET) method.

Metal concentrations were determined using an inductively coupled plasma atomic emission spectroscopy machine (ICP-AES, Optima 7300 DV, Perkin Elmer Co. USA).

We used a portable SG2 SevenGo pH meter (Mettler-Toledo) for pH measurement. The flasks were agitated on a thermostatic mechanical shaker (WNB-14, Memmert).

2.4. Batch sorption experiments

Solutions containing 0.1 g/l of Cd(II) and Zn(II) were prepared using analytical grade cadmium(II)

nitrate nonahydrate and zinc chloride salts, respectively. The effect values of ZnO and CoHCF functionalized with PANI for adsorption of Cd(II) and Zn(II) ions were studied with initial metal concentration 0.1 g/l, 25°C, and in 500 min contact time. The effect of pH of the solution on the Cd^{2+} and Zn^{2+} sorption was studied in the range of 1.5–8.5 and 3.7–7.8, respectively. pH experiment uptake with 0.1 g of dry nanoadsorbents in 20 mL of Cd^{2+} and Zn^{2+} solution. The solution pH was adjusted by 0.1 M KOH or 0.1 M HNO_3. The effect of adsorbent dosage was studied by varying the dose of adsorbent from 1 to 5 g/l on an initial concentration of 0.1 g/l for a contact time of 500 min. For the kinetic experiments, the initial Cd^{2+} and Zn^{2+} ion concentrations used were 0.1 g/l. At various time intervals, samples were collected after filtration and the concentrations of studied pollutants were determined. For examining the effect of initial metal concentration and temperature, the experiments were carried out with an initial metal concentration range of 0.01–0.1 g/l at three different temperatures (25, 40, and 60°C) and after that it was shaken in a thermostatic water bath shaker. After equilibrium was reached, contents were filtered through a filter paper (Whatman 42). The filtrate was analyzed for metal concentration of Cd^{2+} and Zn^{2+} ions using ICP. The amount of metal ions adsorbed onto PANI/CoHCF/NC was calculated by a mass balance relationship, using the following equation:

$$Q_e = (C_i - C_e)\frac{V}{W} \quad (1)$$

where V (L) is the volume, C_i and C_e (g/l) are the initial and final solution concentration of metal ions, respectively, and W (g) is the dry mass of the solid.

The adsorption percentage (AD%) of metal ions was calculated as follows:

$$\text{Adsorption } (\%) = \frac{C_i - C_e}{C_i} \times 100 \quad (2)$$

Within recent decades, linear regression has been one of the most viable tool defining the best fitting relationship [52]. The average absolute value of relative error, (AARE), was used to compare the predicted results with experimental data. This is defined as follows:

$$\text{AARE}\% = \frac{1}{N}\sum_{1}^{N}\frac{\left|q_{e,cal} - q_{e,exp}\right|}{q_{e,exp}} \times 100 \quad (3)$$

in which N is the number of data points [53].

3. Results

3.1. Comparison of the PANI functionalized with ZnO-NPs and CoHCF

3.1.1. Characterization of PANI/CoHCF/NC and PANI/ZnO/NC by FTIR and XRD

The functional groups of samples are characterized by FTIR and the results are shown in Fig. 1. FTIR was used to detect possible structural changes due to the polymerization of polyaniline and composite formation. The samples contain the bare PANI, the PANI/CoHCF/NC, and the PANI/ZnO/NC adsorbents prepared in HCl solution. In both samples, there is a broad bond at around 3,100–3,650 cm^{-1}, which is assigned to O–H stretching for the hydrogen bonded hydroxyl groups which are present in the samples. These active groups can react with Cd^{2+} and Zn^{2+} in aqueous solutions, leading to a large number of adsorption of heavy metal ions. The bands at 1,610 and 1,444 cm^{-1} correspond to quinoid and benzenoid rings, respectively. The bands at 1,286, 1,105, and 788 cm^{-1} correspond to vibrations of C–N bonds in the quinoid and benzenoid rings and to C–H bending in plane or out of plane, respectively. A peak is present at 2,085 cm^{-1}, which is a characteristic peak of the C≡N group. A strong peak at 485 cm^{-1}, which seems to correspond to Zn–O stretching is evident for PANI/ZnO/NC. The shift in the characteristic peaks of PANI/ZnO/NC indicates the presence of interaction between ZnO nanoparticles and molecular chains of PANI. The shift may be ascribed to the formation of hydrogen bonding between ZnO and the NH group of PANI on the surface of ZnO particles [54]. The peak around 2,850–2,950 cm^{-1} is due to the alkyl stretching groups. A Fe–C stretching was seen at 560 cm^{-1} and A Fe–CN–Co peak at 2,090 cm^{-1}, which indicates that CoHCF have been successfully added to the PANI/CoHCF/NC adsorbent.

The XRD analysis was used to determine the structure of the synthesized samples. Fig. 2 depicts the XRD pattern of the bare PANI, PANI/ZnO/NC, and PANI/CoHCF/NC samples. As can be seen, the PANI has an amorphous structure, while PANI/CoHCF/NC has crystal structure.

XRD analysis reveals that the sample obtained can be indexed to the pure cubic structure $Co_3[Fe(CN)_6]_2$. The peaks located at 2θ = 18, 24.8, 35.5, 40.0, 43.9, and 51.0° were assigned to the (2 0 0), (2 2 0), (4 0 0), (4 2 0), (4 2 2), and (4 4 0) reflections of the PANI/CoHCF/NC, respectively [(JCPDS 5-0036, 5-0037)]. No evidence was found for the existence of impurities in the samples.

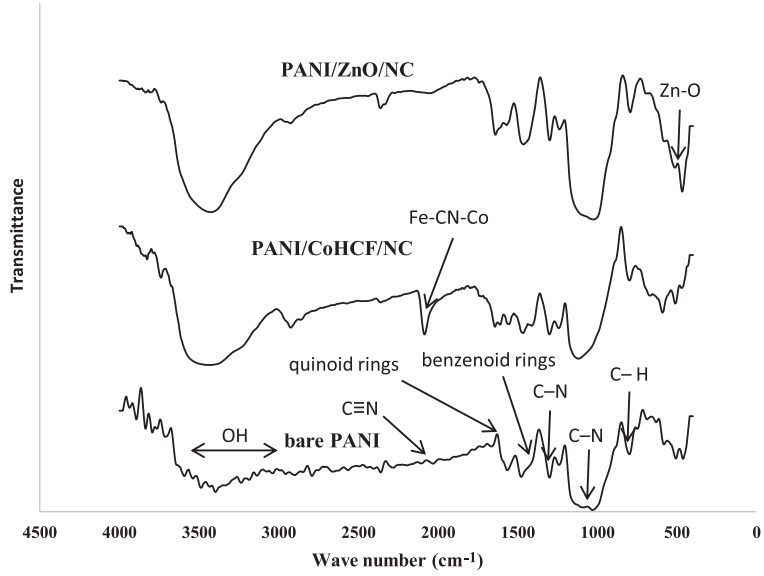

Fig. 1. FTIR spectra of bare PANI, PANI/ZnO/NC, and PANI/CoHCF/NC.

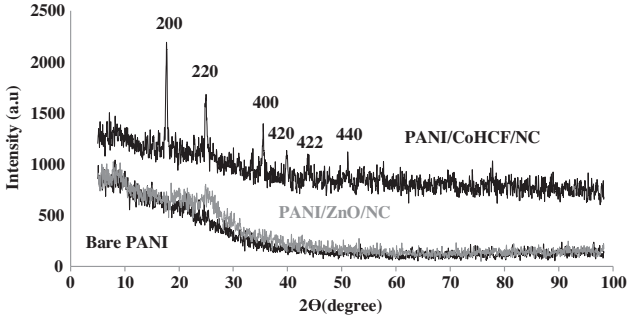

Fig. 2. XRD pattern of the bare PANI, PANI/ZnO/NC, and PANI/CoHCF/NC.

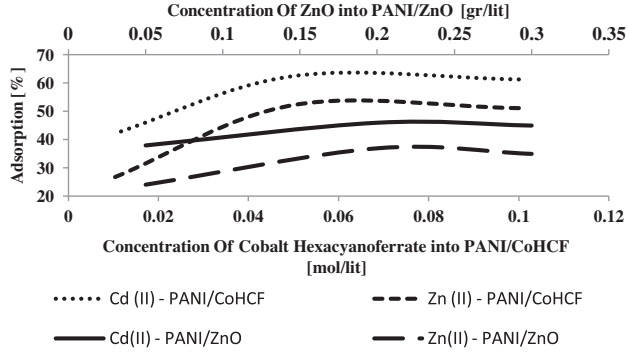

Fig. 3. Comparison and optimization of PANI/CoHCF/NC and PANI/ZnO/NC for adsorption of Cd(II) and Zn (II).

Fig. 2 shows the XRD patterns of pure PANI and PANI/ZnO/NC. This sample showed mainly ZnO with an amorphous background.

3.1.2. Comparison of PANI/CoHCF/NC and PANI/ZnO/NC for adsorption of ions

Concentration of CoHCF in the composite was optimized at 0.01, 0.05, and 0.1 M of Co^{2+} and $K_3[Fe(CN)_6]$. Next, concentration of ZnO in the composite was optimized at 0.05, 0.2, and 0.3 g/l of ZnO. The effects of ZnO and CoHCF onto the functionalized PANI with different concentration of ZnO (g/l) and CoHCF (mol/l) on the adsorption of Cd^{2+} and Zn^{2+} are shown in Fig. 3. As can be seen, the AD% of Cd^{2+} increases with increasing ZnO and CoHCF amount up to 0.22 g/l and 0.07 mol/l, respectively. Also, the AD % of Zn^{2+} increases with increasing ZnO and CoHCF amount up to 0.24 g/l and 0.06 mol/l, respectively. Increasing AD% with the increase in ZnO and CoHCF is due to enhancement of active sites which eases the way of adsorbing Zn^{2+} and Cd^{2+} ions. Reduction in AD% of the PANI/CoHCF/NC and PANI/ZnO/NC for ions sorption of CoHCF and ZnO can be attributed to the agglomeration of CoHCF and ZnO particles which decreases the available surface of adsorption. As we increase the wt% of ZnO in PANI matrix, the possibility of agglomeration of ZnO nanoparticles increases rather than the uniform distribution of ZnO nanoparticles in PANI matrix [54]. On the other hand, the results showed that the AD% of PANI/CoHCF/NC for adsorption of Cd^{2+} and Zn^{2+} is higher than

that of PANI/ZnO/NC adsorbent. The optimum amount of ZnO and CoHCF for removal of Zn^{2+} and Cd^{2+} are shown in Fig. 4. The results showed that the AD% of PANI/CoHCF/NC for adsorption of Cd(II) and Zn(II) is higher than that of PANI/ZnO/NC and the bare PANI. This result is due to attractiveness of CoHCF especially because of excellent properties in capacity to store counter cations and ion-exchange selectivity [55].

From the percentage removal of Cd^{2+} and Zn^{2+} in Fig. 4, it is observed that the metal uptake capacity increases with the presence of cobalt hexacyanoferrate in the composite. It is found that the percentage removal of Cd^{2+} using PANI/CoHCF/NC, PANI/ZnO/NC, and the bare PANI were 64.15, 46, and 35%, respectively. Also the percentage removal of Zn^{2+} using PANI/CoHCF/NC, PANI/ZnO/NC, and the bare PANI were 52.68, 37, and 20%, respectively. These results indicate that cobalt hexacyanoferrate could enhance the adsorption capabilities of PANI. The overall adsorption of Cd^{2+} or Zn^{2+} to the composite increased as compared with that on the bare PANI, because of increasing binding sites on the composites.

So, the further AD% of Cd^{2+} and Zn^{2+} onto the PANI/CoHCF/NC could be attributed to the functional groups of PANI/CoHCF/NC which led to the more available active sites for Cd(II) and Zn(II) sorption in comparison to PANI/CoHCF/NC adsorbent. As a result, PANI/CoHCF/NC is selected for adsorption of metal ions from aqueous solutions for further experiments.

3.2. PANI/CoHCF/NC

3.2.1. Synthesis and characterization of PANI/CoHCF/NC by SEM, TEM, and BET

Synthesis of Prussian blue analogs is as follows: $\boldsymbol{M}_3[Fe(CN)_6]_k$ (***M***etal-HCF) was synthesized by adding 0.03 mol $\boldsymbol{M}Cl_k$ into stoichiometric amount of $K_3[Fe(CN)_6]$ slowly. $\boldsymbol{M}Cl_k{\cdot}6H_2O$ were $FeCl_3$ or $NiCl_2$ or $CoCl_2$[40]. In this paper, $CoCl_2{\cdot}6H_2O$ was used for synthesis of CoHCF.

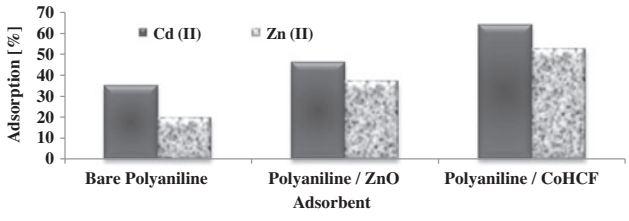

Fig. 4. Comparison of PANI, PANI/CoHCF/NC, and PANI/ZnO/NC for adsorption of Cd(II) and Zn(II).

PANI is generally synthesized by various methods including chemical, electrochemical, and photochemical polymerization. The simplest way for PANI synthesis is the polymerization of aniline with an oxidant such as ammonium peroxydisulfate in an aqueous solution. The polymerization is obtained in an acidic medium [56] such as sulfuric acid [57] and hydrochloric acid [58]. So, chemical synthesis of PANI was carried out in aqueous acid solution using ammonium peroxydisulfate as the oxidant.

The PANI/CoHCF/NC was synthesized via in situ polymerization of aniline monomer in the presence of $(NH_4)_2S_2O_8$ and Co^{2+} and $K_3[Fe(CN)_6]$. The chemical polymerization has advantage of being a simple process capable of producing bulk quantity of PANI. The nanoparticles of cobalt hexacyanoferrate were encapsulated by the precipitating PANI moieties as shown in Fig. 5.

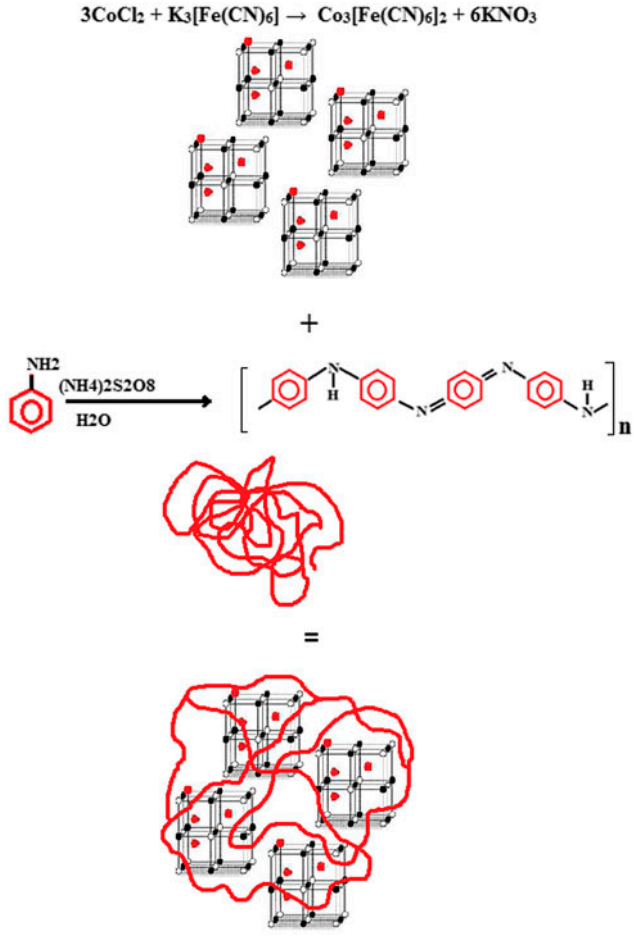

Fig. 5. A schematic representation for formation of the PANI/CoHCF/NC.

The morphology of the products was investigated by TEM and SEM. As Fig. 6(a) shows, the bare PANI sample consisted of capsule surface particles with size of around 75 × 175 nm. The PANI/CoHCF/NC sample consisted of polyhedral particles with size of around 50 nm (Fig. 6(b)). Fig. 6(c), as can be seen the image, confirms the formation of particles on nanoscale with an average size of 20 nm. Also it is clear that the agglomeration of small particles leads to formation of larger particle. The more compact morphology is a result of the polymer growth by instantaneous growth of cobalt hexacyanoferrate, which increases the size of particles significantly. The change in the SEM micrographs of PANI before and after adding CoHCF indicates the structural changes in the adsorbent.

The nitrogen adsorption–desorption isotherms for PANI/CoHCF/NC are shown in Fig. 7. Based on BJH theory, the average pore diameter, the Brunauer–Emmett–Teller (BET) surface area, and the pore volume of PANI/CoHCF/NC are 3.17 nm, 35.21 m^2/g, and 0.2175 cc/g, respectively. Generally, adsorbent pores are classified into three groups: micropores (size < 2 nm), mesopores (2–50 nm), and macropores (size > 50 nm) [59]. So Cd^{2+} and Zn^{2+} diffused in mesopores of PANI/CoHCF/NC.

The isotherms fall within type IV of IUPAC classification group, characteristic of capillary condensation in mesopores indicates that the interaction between adsorptive and adsorbent is higher than interaction between adsorptive and adsorbate. This type of isotherm represents a favorable equilibrium [60].

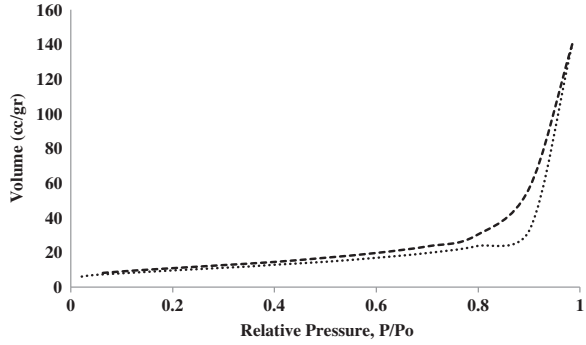

Fig. 7. Nitrogen adsorption–desorption isotherm of the PANI/CoHCF/NC.

As Fig. 7 shows, adsorption hysteresis occurs; it is linked to differences in the adsorption and desorption mechanisms, usually capillary condensation inside mesopores will lead to this phenomenon [61]. The nanocomposite isotherms showed a type H3 hysteresis loop, due to the presence of mesoporosity and narrowslit-shaped pores [62].

The pore size distribution of PANI/CoHCF/NC is shown in Fig. 8. As can be seen, pore diameter of the PANI/CoHCF/NC is in range from 1.17 to 76.51 nm.

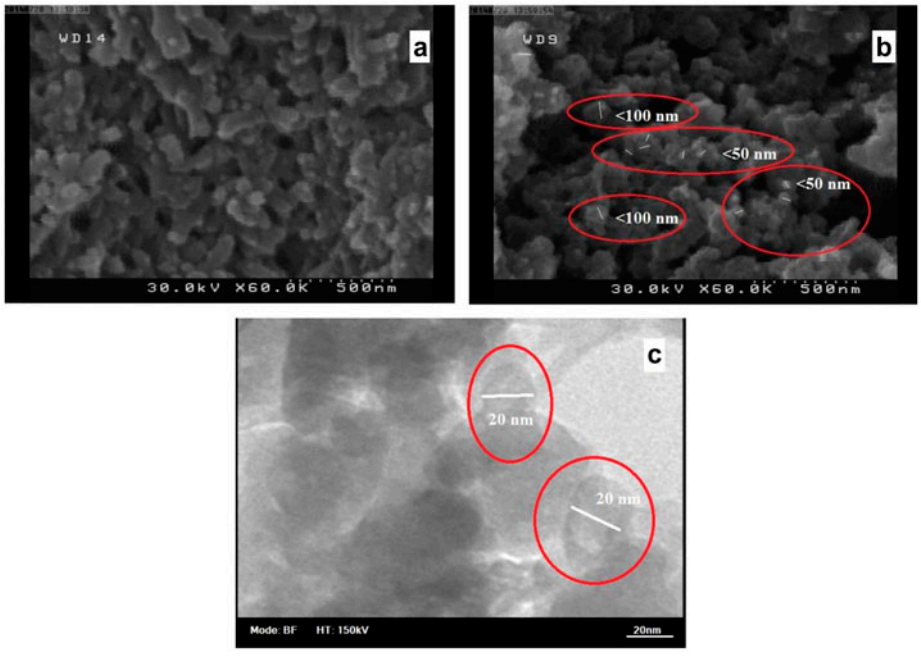

Fig. 6. (a) SEM image of the bare PANI, (b) SEM image of the PANI/CoHCF/NC, and (c) TEM image of the PANI/CoHCF/NC.

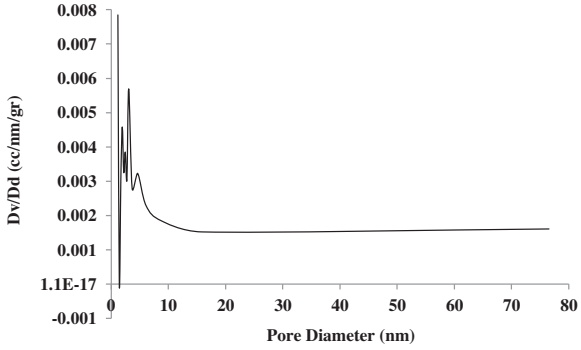

Fig. 8. BJH desorption pore size distribution plot for the PANI/CoHCF/NC.

But the main distribution of pore size was occurred from 1.17 to 4.62 nm. As illustrated on the PANI/CoHCF pore size distribution plot, curves have two main maxima. Two narrow porous volume distributions of 2–3.5 nm were observed, which are large enough to accommodate all the gases and other substances, such as heavy metal ions and drug [39].

3.2.2. Adsorption of Cd^{2+} and Zn^{2+} ions onto PANI/CoHCF/NC

3.2.2.1. Effect of pH. The pH value of the solution is an important controlling parameter in the adsorption process. It is noteworthy that the initial pH value of the solution has more influence than the final pH, which influences both the adsorbent surface metal-binding sites and metal chemistry in the water [63]. At low pH values, the protonation of the anion functional groups of adsorbents reduces the ability of functional group of adsorbents in chelating with metal ions which leads to fewer adsorption capacities of Cd(II) and Zn(II) [64]. Removal of Cd^{2+} from the composite is pH dependent as shown in Fig. 9. At pH < 3, H^+ ions compete with Cd^{2+} ions for the surface of the adsorbent which would hinder Cd(II) ions from reaching the binding sites of the sorbet which is caused by the repulsive forces. This behavior was not changed over the pH range of 3–5. The solubility of cadmium in water is influenced to a large degree by acidity of the water; increase in acidity may lead to dissolving of suspended or sediment-bound cadmium [65]. At pH > 8.0, Cd(II) is precipitated due to formation of cadmium nitrate precipitate by hydroxide anions. The experiment beyond pH 8.0 was not studied because insoluble ion-hydroxide-precipitate was observed in the solution. Removal efficiency of PANI/CoHCF/NC for Cd(II) ion was continuously improved with the increase in pH value from pH 5 to 8.0. Similar results were found for Zn^{2+} ions removal at pH values in the range of 3.7 to 7.5. The trend of removal efficiency was not changed within the pH range of 4.7–6.5 because of lower sorption capacity of the nanocomposite for Zn(II) ions than that of Cd(II) ions. With an increase in pH, the negative charge density of the composite increases due to deprotonation of the metal-binding sites, thus increasing metal sorption. The maximum AD% was of PANI/CoHCF/NC about 80% at pH 7.3.

The negative charges of adsorbent at pH above the zero point charge have strong coordinative affinity toward positively charged metal ions. The degree of surface complexation increases with increasing pH. At pH below the zero point charge, there is a net positive charge on the adsorbent. This enhances the repulsion forces that exist between the positively charged metal ions and the sorbent adsorption sites, therefore decreasing the adsorption [66].

3.2.2.2. Effect of adsorbent dosage. The effect of adsorbent dosage on the adsorption of Cd^{2+} and Zn^{2+} ions is shown in Fig. 10. These data have been obtained at initial metal concentration and temperature equal to 0.1 g/l and 25°C, respectively. This figure illustrates that the adsorbent dosage has an important role in

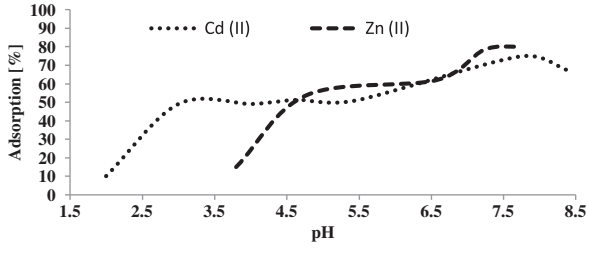

Fig. 9. Effect of pH on the adsorption of Cd(II) and Zn(II) ions onto PANI/CoHCF/NC at 25°C and initial metal concentration: 0.1 g/l.

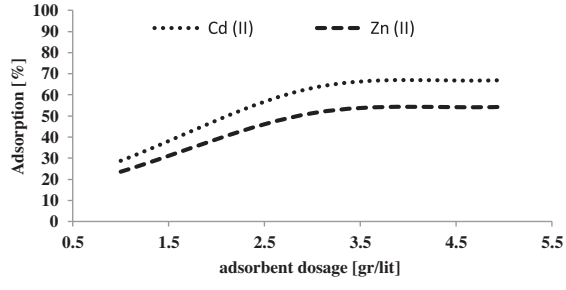

Fig. 10. Effect of adsorbent dosage on the adsorption of Cd (II) and Zn(II) ions onto PANI/CoHCF/NC at 25°C and initial metal concentration: 0.1 g/l.

adsorption processes. Increasing adsorbent dosage has increased Cd^{2+} and Zn^{2+} adsorption to more than 57.1 and 56.8%, respectively.

Fig. 10 illustrates the AD% of Cd^{2+} and Zn^{2+} increase from 1 to 3.5 gr/lit. The increase in the removal efficiency may be attributed to the fact that with an increase in the adsorbent dosage, more adsorbent surface will be available for the adsorbed solute. The AD% of Cd^{2+} and Zn^{2+} reached their maximum values at 3.5 g/l adsorbent dosage.

These data refers to the increase in the AD% with an increase in the adsorbent dosage which is because of higher number of adsorption sites [67] and the availability of further adsorbent surfaces for the solutes to adsorb [68].

3.2.2.3. Effect of contact time and adsorption kinetics. The contact time is one of the most important parameters for economical wastewater treatment applications. Fig. 11 illustrates the AD% of Cd^{2+} and Zn^{2+} metal ions as a function of contact time by initial concentration of 0.1 g/l and at 25°C. It can be noted that the adsorption of all the metals on the adsorbent increases with contact time. As shown in Fig. 11, more than 90% of the total adsorption of metal ions occurs within the first 400 min and the concentrations of Cd^{2+} and Zn^{2+} ions in aqueous solution onto PANI/CoHCF/NC approach their equilibrium value at 500 min. The contact time required for the metal adsorption by this adsorbent is very short compared with other adsorbents such as activated carbon [69] in natural adsorbent group and Fe_3O_4 [34] in nanostructure adsorbent group.

The rapid sorption of ions onto the PANI/CoHCF/NC at the first 400 min is due to a large number of vacant surface sites of adsorbent which are available for the adsorption of metal ions. After 400 min, almost all of the active external sites are saturated, and the adsorption process needs more time to take place by active intraparticle sites. After 500 min, almost all of the internal and external active sites are saturated and the system reaches the sorption equilibrium.

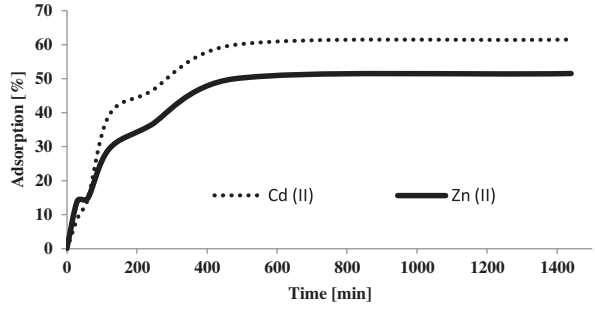

Fig. 11. Effect of contact time on the adsorption of Cd^{2+} and Zn^{2+} ions onto PANI/CoHCF/NC.

Except for adsorption capacity, kinetic performance of a given adsorbent is also of great significance for the pilot applications. From the kinetic analysis, the solute uptake rate, which determines the residence time required for completion of adsorption reaction, is apt to be established. Also, one can make out the scale of an adsorption apparatus based on the kinetic information [70].

Lagergren (1898) presented a first-order rate equation to describe the kinetic process of liquid–solid phase, which is believed to be the earliest model pertaining to the adsorption rate based on the adsorption capacity which is:

$$\frac{dq}{dt} = K_1(q_e - q_t) \tag{4}$$

where q_e and q_t (mg/g) are the adsorption capacities at equilibrium and time t (min), respectively. K_1 (min^{-1}) is the pseudo-first-order rate constant for the kinetic model. Integrating Eq. (4) with the boundary conditions of $q_t = 0$ at $t = 0$ and $q_t = q_t$ at $t = t$, yields [71]:

$$\ln(q_e - q_t) = \ln q_e - K_1 t \tag{5}$$

or

$$q_t = q_e(1 - e^{-K_1 t}) \tag{6}$$

According to Eq. (5), (q_e^b) and (K_1) parameters can be individually calculated from the slope and intercept of the plot of $\ln(q_e - q_t)$ vs. time.

Ho described a kinetic process of the adsorption of divalent metal ions onto peat. Therefore, the adsorbent–metal reaction can be presented as shown in Eqs. (7) and (8), which can be dominant in the adsorption of M^{2+} ions onto adsorbent [72]:

$$2P^- + M^{2+} \leftrightarrow MP_2 \tag{7}$$

$$2HP + M^{2+} \leftrightarrow MP_2 + 2H^+ \tag{8}$$

where P^- and HP are the active sites of the surface.

Therefore, the rate expression can be given as:

$$\frac{dq_t}{dt} = -K_2\left(q_{eq} - q_t\right)^2 \tag{9}$$

Integrating Eq. (9) with the boundary conditions of $q_t = 0$ at $t = 0$ and $q_t = q_t$ at $t = t$, has revealed the linear form of pseudo-second-order rate expression in Eq. (10):

$$\frac{t}{q_t} = \frac{1}{K_2 q_e^2} + \frac{t}{q_e} \tag{10}$$

Or

$$q_t = \frac{K_2 q_e^2 t}{1 + K_2 q_e t} \tag{11}$$

$$h = K_2 q_e^2 \tag{12}$$

Also, h (mg/(g min)) means the initial adsorption rate, and the constants can be determined experimentally by plotting of t/q_t against t.

Both Eqs. (6) and (11) were fitted on experimental data. Fig. 12 shows the agreement between the experimental and calculated data using Eqs. (6) and (11) for the pseudo-first-order kinetic model and pseudo-first-order kinetic models.

The rate constants with models correlation coefficients and R^2 values are given in Table 1. According to Table 1, in the range of 0–500 min, comparing the pseudo-first-and-second-order kinetic models indicates that the adsorption of both ions onto PANI/CoHCF/NC follows readily the pseudo-second-order kinetics. The h parameter shows that Zn(II) has more initial adsorption rate compared with Cd(II).

3.2.2.4. Equilibrium studies in single-component system. In order to explore novel adsorbents in accessing an ideal adsorption system, it is essential to establish the most appropriate adsorption equilibrium correlation, which is indispensable for reliable prediction of adsorption parameters and quantitative comparison of adsorbent behavior for different adsorbent systems (or for different experimental conditions). Equilibrium relationships between adsorbent and adsorbate are described by adsorption isotherms. Usually the relationship between the adsorbed and remaining amount in solution are presented at a fixed temperature. Equilibrium adsorption isotherms are important factors for the design of adsorption systems, and the constants of the isotherms are based on the surface properties and

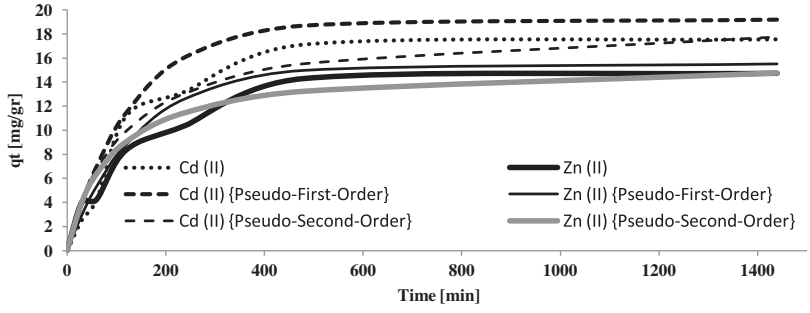

Fig. 12. Pseudo-first-order and pseudo-second-order kinetic models for adsorption of Cd(II) and Zn(II) ions onto PANI/CoHCF/NC.

Table 1
Adsorption kinetic parameters of Cd^{2+} and Zn^{2+} onto PANI/CoHCF/NC at 25°C

Metals	Initial conc., C_i (g/l)	q_e[a] (mg/g)	K_2 (g/mg min)	h (mg/g min)	q_e[b] (mg/g)	R^2
		Pseudo-second-order				
Cd(II)	0.1	17.5714	0.0005	0.1720	19.1205	0.9895
Zn(II)	0.1	14.7143	0.0007	0.1786	15.6495	0.9897
		Pseudo-first order				
		q_e[a] (mg/g)	K_1 (min^{-1})	q_e[b] (mg/g)		R^2
Cd(II)	0.1	17.5714	0.0076	19.2017		0.9808
Zn(II)	0.1	14.7143	0.0070	15.5040		0.9712

[a]Experimental data.
[b]Calculated data.

the capacities of the adsorbents [73]. In general, an adsorption isotherm is an invaluable curve describing the phenomenon governing the retention (or release) or mobility of a substance from the aqueous porous media or aquatic environments to a solid-phase at a constant temperature and pH [74].

Thus, several experiments were carried out to investigate the adsorption isotherm of both metal ions at optimum adsorbent dosage and time by changing the initial concentration of ions in solution in the range of 0.01–0.1 g/l.

Several theoretical and empirical correlations have been reported in the literature for modeling of the adsorption isotherm. The most frequently used models are: Langmuir, Freundlich, Dubinin–Radushkevich, Temkin, Flory–Huggins, Hill, Redlich–Peterson, Sips, Toth, Koble–Corrigan, Radke–Prausnitz, Khan, BET, FHH, and MET.

The Langmuir isotherm assumes monolayer adsorption (the adsorbed layer is one molecule in thickness) on homogenous sites. Adsorption can only occur at a finite (fixed) number of definite localized sites that are identical and equivalent with no lateral interaction and steric hindrance between the adsorbed molecules, even on adjacent sites [75]. It is expressed as:

$$q_e = \frac{q_{max} K_L C_e}{1 + K_L C_e} \tag{13}$$

Linear regression was the easy and practical way of curve fitting when it was first suggested several decades ago, but it has become a customary principle nowadays and is still widely used in spite of the availability of microcomputers and advanced statistical softwares. The linear equation of the Langmuir isotherm model is:

$$\frac{C_e}{q_e} = \frac{1}{q_{max} K_L} + \frac{C_e}{q_{max}} \tag{14}$$

where C_e is the equilibrium concentration (g/l), q_e the amount adsorbed (mg/g), q_{max} is the monolayer adsorption capacity of the adsorbent (mg/gr), and K_L is the Langmuir constant (l/mg) related to the free energy of adsorption. According to Eq. (14), (q_{max}) and (K_L) parameters can be individually calculated from the slope and intercept of the plot of (C_e/q_e) vs. C_e.

The shape of the isotherm may also be considered to be predicted if an adsorption system is "favorable" or "unfavorable". The essential characteristic of a Langmuir isotherm can be expressed in terms of a dimensionless "separation factor" (R_L), which is defined by the following equation:

$$R_L = \frac{1}{1 + C_i K_L} \tag{15}$$

where K_L (l/mg) refers to the Langmuir constant and C_i denotes to the adsorbate initial concentration (g/l). In this context, lower R_L value reflects that adsorption is more favorable. In a detailed explanation, R_L value indicates the adsorption nature to be either unfavorable ($R_L > 1$), linear ($R_L = 1$), favorable ($0 < R_L < 1$), or irreversible ($R_L = 0$) [76].

The equilibrium isotherms for the adsorption of metal ions in single-solute systems by PANI/CoHCF/NC at 25–60˚C are presented in Figs. 13 and 14.

The values of R_L for cadmium and zinc have been calculated as 0.089–0.608 and 0.014–0.475, respectively. Hence, the adsorption of Cd^{2+} and Zn^{2+} onto PANI/CoHCF/NC are favorable. It is noteworthy that 0.089 and 0.014 are for maximum initial metal concentrations (0.1 g/l) at maximum temperature (60˚C). Also, 0.608 and 0.475 are for minimum initial metal concentration (0.01 g/l) at minimum temperature (25˚C). It goes without saying that R_L (favorable) decreases with an increase in initial metal ion concentration (driving force) and temperature (Fig. 15).

Fig. 15 illustrates that the favorable data of Cd^{2+} in all temperatures at constant initial concentration is higher than Zn^{2+} due to increase in K_L (Langmuir constant) of Cd^{2+}.

The empirical Freundlich model can be applied to non-ideal sorption and reversible adsorption, on heterogeneous surfaces and multilayer sorption (not restricted to the formation of monolayer). The Freundlich model in linear form is given as follows [77]:

$$q_e = K_F C^{\frac{1}{n}} \tag{16}$$

The linear equation of the Freundlich isotherm model is:

$$\log q_e = \log K_F + \frac{1}{n} \log C_e \tag{17}$$

where C_e is the equilibrium concentration (g/l), q_e is the amount adsorbed (mg/g), q_{max} is the monolayer adsorption capacity of the adsorbent (mg/g), K_F is related to the adsorption capacity, and $1/n$ is an empirical parameter related to the adsorption intensity, which varies with the heterogeneity of material. According to Eq. (17), ($1/n$) and (K_F) parameters can be individually calculated from the slope and intercept of the plot of ($\log q_e$) vs. ($\log C_e$). $1/n$ values indicate the type of isotherm to be irreversible ($1/n = 0$), favorable ($0 < 1/n < 1$), unfavorable ($1/n > 1$) [78].

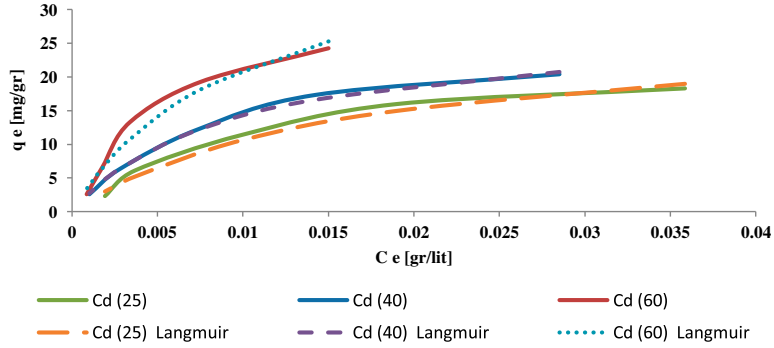

Fig. 13. Langmuir isotherm model of Cd^{2+} ion adsorption onto PANI/CoHCF/NC.

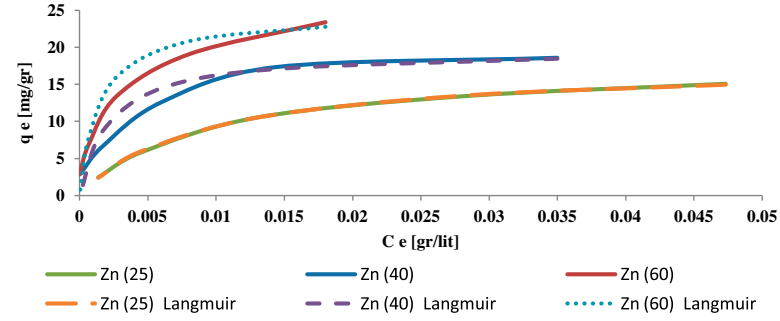

Fig. 14. Langmuir isotherm model of Zn^{2+} ion adsorption onto PANI/CoHCF/NC.

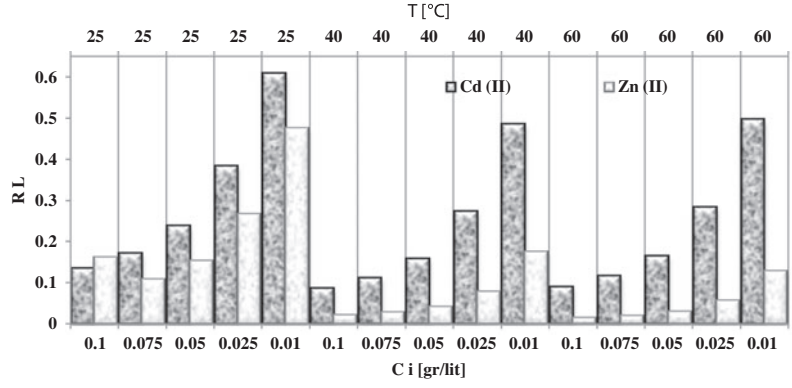

Fig. 15. R_L parameter of Langmuir isotherm model on the adsorption of Cd(II) and Zn(II) ions onto PANI/CoHCF/NC at 25, 40, and 60°C and initial metal concentration: 0.1, 0.07, 0.05, 0.02, and 0.01 g/l.

Figs. 16 and 17 show the comparison of experimental data of Cd(II) and Zn(II) ions with the q_e values obtained by applying Eq. (13).

Dubinin–Radushkevich isotherm is generally described as the adsorption mechanism with a Gaussian energy distribution onto heterogeneous surface [79]. The D–R isotherm is expressed as:

$$q_e = (q_s)e^{(-K_{ad}\varepsilon^2)} \tag{18}$$

$$\ln q_e = \ln q_s - (K_{ad}\varepsilon^2) \tag{19}$$

where q_e is amount of adsorbate in the adsorbent at equilibrium (mg/g), q_s is the theoretical isotherm

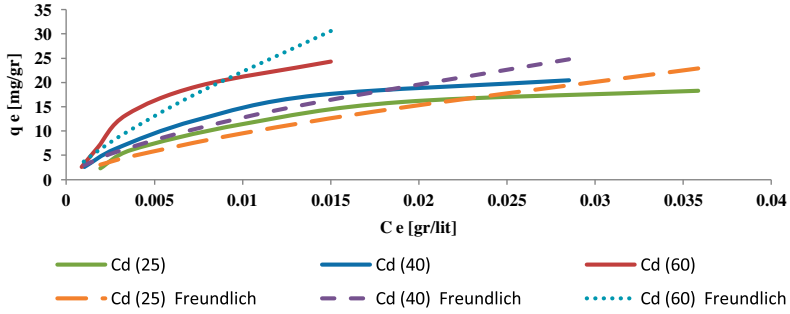

Fig. 16. Freundlich isotherm model of Cd^{2+} ion adsorption onto PANI/CoHCF/NC.

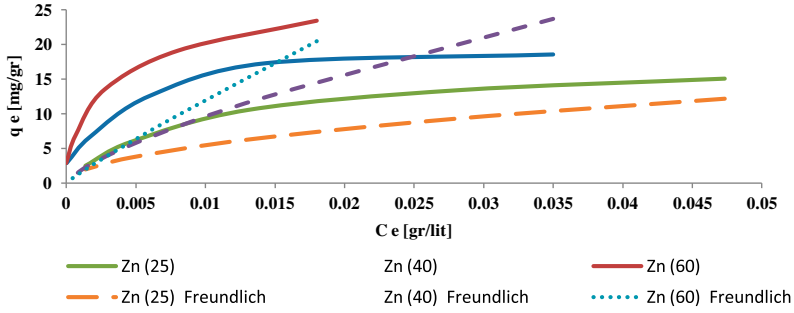

Fig. 17. Freundlich isotherm model of Zn^{2+} ion adsorption onto PANI/CoHCF/NC.

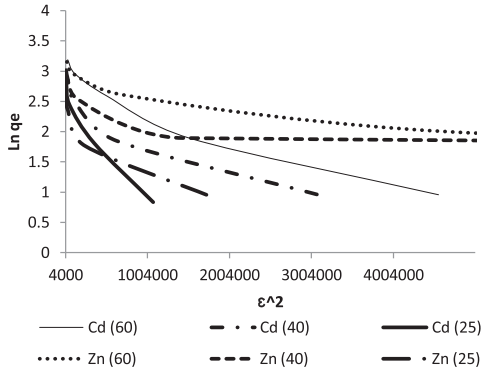

Fig. 18. $\ln(q_e)$ vs. ε^2.

saturation capacity (mg/g), K_{ad} is the Dubinin–Radushkevich isotherm constant (mol^2/kJ^2) and ε is the Dubinin–Radushkevich isotherm constant (Polanyi Potential). The approach was used to distinguish the physical and chemical adsorption of Cd(II) and Zn(II) with its free energy (E) of sorption per molecule of the sorbate when it is transferred to the surface of the solid from infinity in solution (Eq. (20)):

$$E = \left[\frac{1}{\sqrt{2B_{DR}}}\right] \tag{20}$$

where B_{DR} is denoted as the isotherm constant and ε is equal to Eq. (21):

$$\varepsilon = RT \ln\left[1 + \frac{1}{C_e}\right] \tag{21}$$

where R is the gas constant (8.314 J/mol K), T is absolute temperature (K), and C_e is adsorbate equilibrium concentration (g/l). Due to the experiments performed at different temperatures and D–R isotherm is temperature-dependent, D–R isotherm fitting can be used for these materials. In order to achieve this goal, adsorption data at different temperatures was plotted of ln (q_e) vs. ε^2 by applying Eq. (19) (Fig. 21).

Figs. 19 and 20 show the comparison of experimental data of Cd(II) and Zn(II) ions with the q_e values obtained by applying Eq. (18).

It can be seen that the increase in adsorption capacity with an increase in equilibrium metal ion concentration for different metal ions is in the order of $Cd^{2+} > Zn^{2+}$. Adsorption capacity increases by increasing the initial concentration in metal ions. With further increase of initial concentration of metal ions, adsorption capacity reaches a constant value due to saturation of the active sites of the adsorbent. Adsorption increases uptake due to greater availability of active

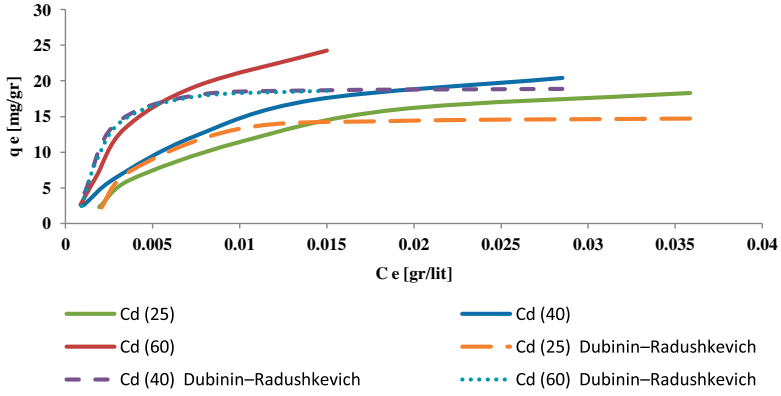

Fig. 19. Dubinin–Radushkevich isotherm model of Cd^{2+} ion adsorption onto PANI/CoHCF/NC.

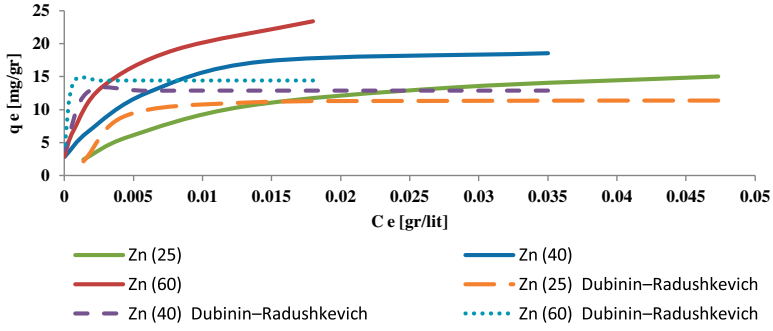

Fig. 20. Dubinin–Radushkevich isotherm model of Zn^{2+} ion adsorption onto PANI/CoHCF/NC.

sites of adsorbent for chelating with metal ions. This can be seen in all experimental temperatures and it means that in isothermal conditions, with increasing initial metal ion concentration, the absorption capacity increases to reach a q_{max}.

Correlation coefficients, R^2, AARE%, and experimental data with the q_e values obtained by applying Eqs. (13)–(21) are reported in Table 2.

From R^2 and ARRE% values in Table 2, it is clear that the Langmuir model predicts experimental data better than Freundlich and D–R isotherm models. This result means that the adsorbent surface is homogeneous with equal energy in its site and adsorbent sites are homogeneously distributed all over the adsorbent.

By fitting the experimental results to the Langmuir isotherms model, it is found that the maximum uptake for Cd^{2+} at 25, 40, and 60°C using PANI/CoHCF/NC were 27.174, 27.548, and 41.841 mg/g, respectively. Also for Zn^{2+} at 25, 40, and 60°C using PANI/CoHCF/NC were 17.857, 19.608, and 24.631 mg/g, respectively. K_L values of Cd^{2+} and Zn^{2+} by PANI/CoHCF/NC are in decreasing order, showing the order of metal affinity.

A comprehensive coverage of different adsorbents under different environmental conditions can be found in the format of several publications. It is observable that q_m values differ widely for different adsorbents. Based on Table 3, it can be concluded that PANI/CoHCF/NC exhibits moderate adsorption capacity for Cd^{2+} and Zn^{2+}.

Though the performance of this adsorbent is comparable with that of other adsorbents, cost comparisons are difficult to make due to scarcity of consistent cost information in the literature data [66].

3.2.2.5. Effect of temperature and adsorption thermodynamics. To study the effect of temperature, adsorption experiments were carried out from 25C to 60°C in 20 mL of metal ion (Cd^{2+} or Zn^{2+}) solutions with initial concentration of 10–0.1 g/l (Figs. 13, 14, and 16–20). The AD% increased with increasing temperature from 25 to 60°C. Fig. 21 shows endothermic nature of the adsorption process which was later utilized for determination of changes in thermodynamic parameters such as Gibbs free energy (ΔG°), heat of adsorption (ΔH°), and entropy (ΔS°) of the sorption of

Table 2
Adsorption isotherm parameters for Cd^{2+} and Zn^{2+} ions onto PANI/CoHCF/NC in single-component system

	25 °C				40 °C				60 °C			
Langmuir isotherm model												
	q_m	K_L	R^2	AARE%	q_m	K_L	R^2	AARE%	q_m	K_L	R^2	AARE%
Cd^{2+}	27.174	0.064	0.943	12.355	27.548	0.106	0.997	2.579	41.841	0.101	0.879	12.398
Zn^{2+}	17.857	0.110	1.000	1.587	19.608	0.472	0.991	28.693	24.631	0.684	0.983	29.008
Freundlich isotherm model												
	$1/n$	K_F	R^2	AARE%	$1/n$	K_F	R^2	AARE%	$1/n$	K_F	R^2	AARE%
Cd^{2+}	0.686	1.961	0.920	20.786	0.636	2.944	0.964	14.175	0.770	3.809	0.928	20.034
Zn^{2+}	0.515	1.672	0.965	29.461	0.727	1.787	0.958	52.229	0.913	1.464	0.900	63.736
Dubinin–Radushkevich												
	K^{ad} (mol^2/kJ^2)	q^s (mg/gr)	E	AARE%	K^{ad} (mol^2/kJ^2)	q^s (mg/gr)	E	AARE%	K^{ad} (mol^2/kJ^2)	q^s (mg/gr)	E	AARE%
Cd^{2+}	2E−6	14.878	500	18.044	1E−6	18.948	1,000	47.222	5E−7	18.948	1,000	19.936
Zn^{2+}	9E−7	11.403	745	22.439	1E−8	12.900	7,071	37.061	2E−9	14.402	15,811	42.390

Cd(II) and Zn(II) from aqueous solutions. The increase in sorption with the rise in temperature, to the best of our knowledge, is due to the strengthening of adsorptive forces between the active sites of the PANI/CoHCF/NC and adsorbate species and between the adjacent molecules of the adsorbed phase [51].

Changes in standard Gibbs free energy for the adsorption process were evaluated using K_L values obtained from the Langmuir model at different temperatures [86]. K can be expressed as $K_L \times C_s$, where K_L is the equilibrium Langmuir constant and C_s is the solvent molar concentration, which can be calculated from the density and molecular weight of water at the given temperature [87]. To study the thermodynamics of adsorption of Cd^{2+} and Zn^{2+} on PANI/CoHCF/NC, thermodynamic constants were calculated using the following equations:

$$\ln K = \frac{\Delta S^\circ}{R} - \frac{\Delta H^\circ}{RT} \tag{22}$$

$$\Delta G^\circ = -RT \ln K \tag{23}$$

$$\Delta G^\circ = \Delta H^\circ - T\Delta S^\circ \tag{24}$$

where R (8.314 J/mol/K) is the gas constant and T (K) the absolute temperature. According to Eq. (22), $(-\Delta H^\circ/R)$ and $(\Delta S^\circ/R)$ parameters can be individually calculated from the slope and intercept of the plot of $(\ln K)$ vs. $(1/T)$ (Fig. 22).

The thermodynamic parameters of Cd(II) and Zn (II) ions adsorption on PANI/CoHCF/NC at 313, 313, and 333 K are shown in Table 4.

The calculated values of ΔS° and ΔH° for Cd^{2+} were 109.3351 J/(mol K) and 10.2525 J/mol, respectively. Also for Zn^{2+} ions they were 217.1238 J/(mol K) and 42.1343 J/mol, respectively. A perusal of Table 4 reveals that the enthalpy change (ΔH°) is positive (endothermic) owing to an increase in adsorption aligned with a successive increase in temperature.

The mechanism of adsorption of Cd^{2+} and Zn^{2+} on PANI/CoHCF/NC uptakes in the several main steps [88]: (a) diffusion of ions from the bulk of solution to the film surrounding the nano-particle. (b) Diffusion of ions through the external film (external surface of the adsorbent). (c) Particle diffusion through the pores toward the adsorptive sites. (d) Dehydration of Cd^{2+} and Zn^{2+} in the proximity of adsorptive sites and hydration of the counterbalance cations (counter ions of the PANI/CoHCF/NC). (e) The inversion phenomenon between the ions and counterbalance cations. (f) Binding of ions on the active sites.

Table 3
Comparison of maximum adsorption capacity of PANI/CoHCF/NC with those of some other adsorbents reported in literature for Cd^{2+} and Zn^{2+} adsorption

Adsorbent	Maximum adsorbed amount, q_{max} (mg/g)		Refs.
	Cd(II)	Zn(II)	
Eggshell	3	–	[80]
Expanded perlite	1.79	–	[81]
Rice bran	1	0.1	[82]
Sawdust	–	2	[83]
Fe_3O_4 nanoparticle	–	0.16	[34]
Dithizone-anchored poly (EGDMA-HEMA) microbeads	–	4.3	[84]
Fe_3O_4@APS@AA-co-CA MNPs	29.6	43.4	[85]
Fe_3O_4–cyclodextrin polymer nanocomposites	27.7	–	[66]
PANI/CoHCF/NC	27.17	17.85	This study

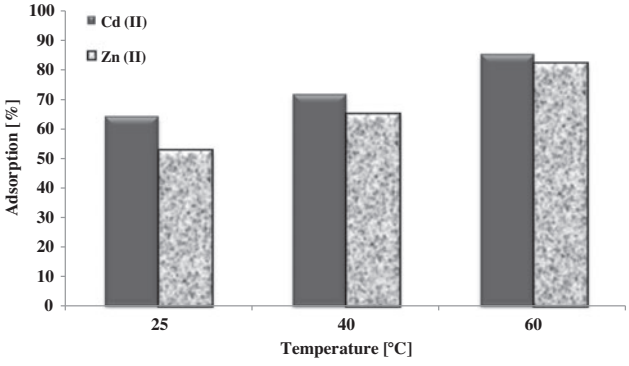

Fig. 21. Effect of temperature on the adsorption of Cd^{2+} and Zn^{2+} ions onto PANI/CoHCF/NC at 25, 40, and 60°C and initial metal concentration: 0.1 g/l.

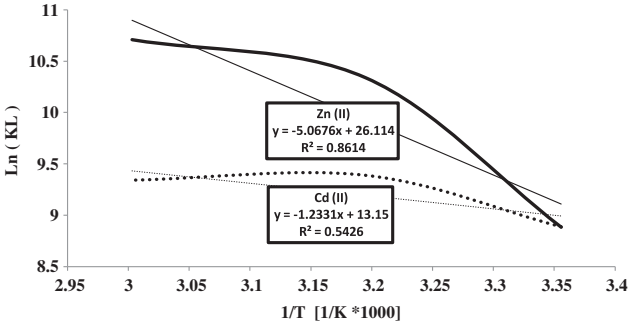

Fig. 22. $\ln K$ vs. $1/T$ for estimation of ΔH° and ΔS° for Cd^{2+} and Zn^{2+} ions onto PANI/CoHCF/NC.

(g) Diffusion of counter ions along the same path back to the bulk of solution.

As can be seen, some of steps are endothermic and some of other steps are exothermic. Dehydration of Cd^{2+} and Zn^{2+} is an endothermic process, while binding of ions on the active sites is an exothermic process. So, when the ΔH° is positive (endothermic), the energy of dehydration of Cd^{2+} and Zn^{2+} is greater than the energy of binding.

The negative ΔG° values indicated thermodynamical feasibility and spontaneous nature of the adsorption. Also higher negative Gibbs free energy at higher temperatures suggests that the inclination toward the spontaneous nature of reaction is stronger at higher temperatures. The positive value of ΔS° reveals the increased randomness at the solid–solution interface during the fixation of ion on adsorbent surface [89]. Increased randomness at the solid–solution occurred with enhanced the diffusion of counter ions of adsorbent to the external solution. Also, when one ion (Cd^{2+} or Zn^{2+}) bound on the active sites, two ions (K^+) was being released to the external solution. This is the reason of increased randomness.

3.2.2.6. Adsorption mechanism. The removal of Cd^{2+} and Zn^{2+} by cobalt hexacyanoferrates composite includes adsorption and sorption processes. The word "sorption" as used here, is relative to any process involving the transfer of species dissolved in a solution to a solid immersed within the solution. The sorption process depends on the crystal structure of the solid, along with the size and charge of the ions. The sorption process may be a phase transformation or a true ion exchange. These different mechanisms lead to different sorption kinetics, capacities, and stability of sorbent particles. In the case of cobalt hexacyanoferrate, the sorption of Cd^{2+} and Zn^{2+} seems to proceed with the exchange by the intercalated alkali ions. The actual chemical composition of our product is $K_xCo_y[Fe(CN)_6]_2$ (where $x \approx 0.001$ and $y \approx 3$). This formulation is very close to the stoichiometric formula

Table 4
Thermodynamic parameters for adsorption of Cd^{2+} and Zn^{2+} ions onto PANI/CoHCF/NC

	T (K)	K_c	ΔS° (J/mol K)	ΔH° (J/mol)	ΔG° (J/mol)
Cd(II)	298	7,233.24	109.3351	10.2525	−32,571.621
	313	11,955.71	109.3351	10.2525	−34,211.649
	333	11,403.22	109.3351	10.2525	−36,398.352
Zn(II)	298	7,214.03	217.1238	42.1343	−64,660.760
	313	30,878.61	217.1238	42.1343	−67,917.617
	333	44,694.18	217.1238	42.1343	−72,260.093

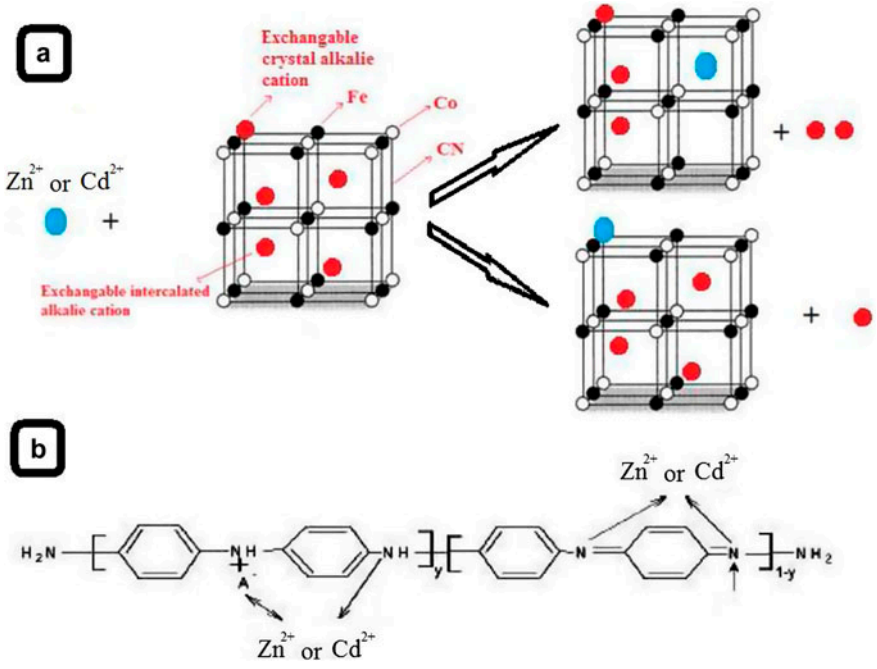

Fig. 23. Ion sorption process by (a) cobalt hexacyanoferrate and (b) PANI.

$Co_3[Fe(CN)_6]_2$. Therefore, some of the alkali ions are located in crystal sites and some of them are kept in the internal spaces of crystal. The presence of alkali ions in the product induces ion-exchange properties of it by the two following mechanisms (Fig. 23(a)).

$$\mathbf{M}^{2+} + K_2Co_3[Fe(CN)_6] \rightarrow \mathbf{M}Co_3[Fe(CN)_6] + 2K^+_{crystal};\quad \mathbf{M} = \text{Cd or Zn} \tag{25}$$

$$\mathbf{M}^{2+} + K_2Co_3[Fe(CN)_6] \rightarrow \mathbf{M}Co_3[Fe(CN)_6] + 2K^+_{trapped};\quad \mathbf{M} = \text{Cd or Zn} \tag{26}$$

Fig. 23(b) shows the possible mechanism for Cd^{2+} or Zn^{2+} adsorption on PANI. It is widely accepted that nitrogen-containing functional groups can act as adsorption sites for metal ions. Adsorption isotherms confirmed that the removal of Cd^{2+} or Zn^{2+} occurs by chemisorption in monolayer fashion on the surfaces of polyaniline. The overall adsorption of Cd^{2+} or Zn^{2+} to the composite increased as compared with that on the simple polyaniline, because of the availability of more binding sites on the composites.

4. Conclusion

The effects of ZnO and CoHCF onto the functionalized PANI with different concentration of ZnO (g/l) and CoHCF (mol/l) on the adsorption of Cd^{2+} and Zn^{2+} were investigated. The results showed that the AD% of PANI/CoHCF/NC for adsorption of Cd^{2+} and Zn^{2+} is higher than PANI/ZnO/NC and the bare PANI adsorbents. So, PANI/CoHCF/NC is selected

for adsorption of metal ions from aqueous solutions for further experiments.

The results of BET analysis showed that Cd^{2+} and Zn^{2+} diffused in mesopores PANI/CoHCF/NC. The change in the SEM micrographs of PANI before and after adding CoHCF indicates the structural changes in the adsorbent. The TEM image of the PANI/CoHCF/NC has been shown. The image confirmed the formation particles in nanoscale with average size of 20 nm. The optimum condition for adsorption of Cd^{2+} and Zn^{2+} onto the PANI/CoHCF/NC in a batch mode was found to be at 3.5 g/l adsorbent dosage. The maximum AD% was of PANI/CoHCF/NC about 80% at pH 7.3. The kinetic data were found to follow pseudo-second-order kinetic model and the equilibrium time was obtained after 500 min. The comparison of isotherm models showed that the Langmuir model describes the equilibrium data of Cd^{2+} and Zn^{2+} sorption better than another.

References

[1] M. Ghaedi, M. Montazerozohori, S. Heidarpour, H.R. Noormohamadi, A. Asghari, M. Soylak, Physical modification of palladium and silver nanoparticles loaded on activated carbon with 2-(2-Nitrobenzylideneamino) thiophenol to preconcentrate and separate metal ions from food samples, Fresenius Environ. Bull. 22 (2013) 3343–3351.

[2] H. Duan, J. Wang, Z. Huang, B. Karihaloo, Size-dependent effective elastic constants of solids containing nano-inhomogeneities with interface stress, J. Mech. Phys. Solids 53 (2005) 1574–1596.

[3] M. Roosta, M. Ghaedi, A. Daneshfar, R. Sahraei, Ultrasound assisted microextraction-nano material solid phase dispersion for extraction and determination of thymol and carvacrol in pharmaceutical samples: Experimental design methodology, J. Chromatogr. B 975 (2015) 34–39.

[4] S. Salem, A. Salem, A.A. Babaei, Application of Iranian nano-porous Ca-bentonite for recovery of waste lubricant oil by distillation and adsorption techniques, J. Ind. Eng. Chem. 23 (2014) 154–162.

[5] X. Chen, H. Schluesener, Nanosilver: A nanoproduct in medical application, Toxicol. Lett. 176 (2008) 1–12.

[6] W. Zhu, P. Bartos, A. Porro, Application of nanotechnology in construction, Mater. Struct. 37 (2004) 649–658.

[7] C.-S. Jwo, H. Chang, H.-M. Lin, T. Kupka, W.-A. Chiou, Nano, ceramic, and metallic materials for energy application, Adv. Mater. Sci. Eng. 2014 (2014), Article ID 367263, 2 pp.

[8] H. Presting, U. König, Future nanotechnology developments for automotive applications, Mater. Sci. Eng.: C 23 (2003) 737–741.

[9] N. Sozer, J.L. Kokini, Nanotechnology and its applications in the food sector, Trends Biotechnol. 27 (2009) 82–89.

[10] M. Ghaedi, K. Niknam, S. Zamani, H.A. Larki, M. Roosta, M. Soylak, Silica chemically bonded N-propyl kriptofix 21 and 22 with immobilized palladium nanoparticles for solid phase extraction and preconcentration of some metal ions, Mater. Sci. Eng.: C 33 (2013) 3180–3189.

[11] G.M. Irvine, J.M. Blais, J.R. Doyle, L.E. Kimpe, P.A. White, Cancer risk to First Nations' people from exposure to polycyclic aromatic hydrocarbons near in-situ bitumen extraction in Cold Lake, Alberta, Environ. Health 13 (2014) 7.

[12] J.M. Matés, J.A. Segura, F.J. Alonso, J. Márquez, Roles of dioxins and heavy metals in cancer and neurological diseases using ROS-mediated mechanisms, Free Rad. Biol. Med. [Review] 49 (2010) 1328–1341.

[13] S.T. Glassmeyer, E.T. Furlong, D.W. Kolpin, J.D. Cahill, S.D. Zaugg, S.L. Werner, M.T. Meyer, D.D. Kryak, Transport of chemical and microbial compounds from known wastewater discharges: Potential for use as indicators of human fecal contamination, Environ. Sci. Technol. 39 (2005) 5157–5169.

[14] P. Govil, J. Sorlie, D. Sujatha, A. Krishna, N. Murthy, K.R. Mohan, Assessment of heavy metal pollution in lake sediments of Katedan Industrial Development Area, Hyderabad, India, Environ. Earth Sci. 66 (2012) 121–128.

[15] V.K. Garg, P. Yadav, S. Mor, B. Singh, V. Pulhani, Heavy metals bioconcentration from soil to vegetables and assessment of health risk caused by their ingestion, Biol. Trace Elem. Res. 157 (2014) 256–265.

[16] N. Kamel, T. Burgeot, M. Banni, M. Chalghaf, S. Devin, C. Minier, H. Boussetta, Effects of increasing temperatures on biomarker responses and accumulation of hazardous substances in rope mussels (*Mytilus galloprovincialis*) from Bizerte lagoon, Environ. Sci. Pollut. Res. 21 (2014) 6108–6123.

[17] C. Vázquez-Boucard, G. Anguiano-Vega, L. Mercier, E. Rojas del Castillo, Pesticide residues, heavy metals, and DNA damage in sentinel oysters *Crassostrea gigas* from Sinaloa and Sonora, Mexico, J. Toxicol. Environ. Health, Part A 77 (2014) 169–176.

[18] L. Marder, A.M. Bernardes, J. Zoppas Ferreira. Cadmium electroplating wastewater treatment using a laboratory-scale electrodialysis system, Sep. Purif. Technol. 37 (2004) 247–255.

[19] A. Vaněk, L. Borůvka, O. Drábek, M. Mihaljevič, M. Komárek, Mobility of lead, zinc and cadmium in alluvial soils heavily polluted by smelting industry, Plant, Soil Environ. 51 (2005) 316–321.

[20] A. Kumar, P. Pastore, Lead and cadmium in soft plastic toys, Curr. Sci. 93 (2007) 818–822.

[21] M.M.B. Paoliello, E.M. De Capitani, F.G. da Cunha, T. Matsuo, M.d.F. Carvalho, A. Sakuma, B.R. Figueiredo, Exposure of children to lead and cadmium from a mining area of Brazil, Environ. Res. 88 (2002) 120–128.

[22] Z. Yanqun, L. Yuan, C. Jianjun, C. Haiyan, Q. Li, C. Schvartz, Hyperaccumulation of Pb, Zn and Cd in herbaceous grown on lead–zinc mining area in Yunnan, China, Environ. Int. 31 (2005) 755–762.

[23] R. Subbiah, C. Sastry, P. Agamuthu, Removal of zinc from rubber thread manufacturing industry wastewater using chemical precipitant/flocculant, Environ. Prog. 19 (2000) 299–304.

[24] M.P. Waalkes, Cadmium carcinogenesis in review, J. Inorg. Biochem.. 79 (2000) 241–244.
[25] T. Nawrot, M. Plusquin, J. Hogervorst, H.A. Roels, H. Celis, L. Thijs, J. Vangronsveld, E. Van Hecke, J.A. Staessen, Environmental exposure to cadmium and risk of cancer: A prospective population-based study, Lancet Oncol. 7 (2006) 119–126.
[26] T. Caciari, A. Sancini, M. Fioravanti, A. Capozzella, T. Casale, L. Montuori, M. Fiaschetti, M.P. Schifano, G. Andreozzi, N. Nardone, Cadmium and hypertension in exposed workers: A meta-analysis, Int. J. Occup. Med. Environ. Health 26 (2013) 440–456.
[27] M. Ghaedi, M. Montazerozohori, M. Sajedi, M. Roosta, M.N. Nickoosiar Jahromi, A. Asghari, Comparison of novel sorbents for preconcentration of metal ions prior to their flame atomic absorption spectrometry determination, J. Ind. Eng. Chem. 19 (2013) 1781–1787.
[28] F. Fu, Q. Wang, Removal of heavy metal ions from wastewaters: A review, J. Environ. Manage. 92 (2011) 407–418.
[29] F. Lin, D. Liu, S. Maiti Das, N. Prempeh, Y. Hua, J. Lu, Recent Progress in heavy metal extraction by supercritical CO_2 fluids, Ind. Eng. Chem. Res. 53 (2014) 1866–1877.
[30] H. Ali, E. Khan, M.A. Sajad, Phytoremediation of heavy metals—Concepts and applications, Chemosphere 91 (2013) 869–881.
[31] N. Ballav, H.J. Choi, S.B. Mishra, A. Maity, Synthesis, characterization of Fe_3O_4@glycine doped polypyrrole magnetic nanocomposites and their potential performance to remove toxic Cr(VI), J. Ind. Eng. Chem. 20 (2014) 4085–4093.
[32] A.A. Farghali, M. Bahgat, A. Enaiet Allah, M.H. Khedr, Adsorption of Pb(II) ions from aqueous solutions using copper oxide nanostructures, beni-seuf univ, J. Appl. Sci. 2 (2013) 61–71.
[33] A.R. Türker, New Sorbents for Solid-Phase Extraction for Metal Enrichment, Clean—Soil, Air, Water 35 (2007) 548–557.
[34] L. Giraldo, A. Erto, J.C. Moreno-Piraján, Magnetite nanoparticles for removal of heavy metals from aqueous solutions: Synthesis and characterization, Adsorption 19 (2013) 465–474.
[35] M. Berrettoni, M. Giorgetti, S. Zamponi, P. Conti, D. Ranganathan, A. Zanotto, M.L. Saladino, E. Caponetti, Synthesis and characterization of nanostructured cobalt hexacyanoferrate, J. Phys. Chem. C 114 (2010) 6401–6407.
[36] M. Pyrasch, A. Toutianoush, W. Jin, J. Schnepf, B. Tieke, Self-assembled films of Prussian Blue and analogues: Optical and electrochemical properties and application as ion-sieving membranes, Chem. Mater. 15 (2003) 245–254.
[37] F. Ricci, G. Palleschi, Sensor and biosensor preparation, optimisation and applications of Prussian Blue modified electrodes, Biosens. Bioelectron. 21 (2005) 389–407.
[38] P.K. Thallapally, R.K. Motkuri, C.A. Fernandez, B.P. McGrail, G.S. Behrooz, Prussian Blue analogues for CO_2 and SO_2 capture and separation applications, Inorg. Chem. 49 (2010) 4909–4915.
[39] L. Hu, P. Zhang, Q.-W. Chen, J.-Y. Mei, N. Yan, Room-temperature synthesis of Prussian blue analogue $Co_3[Co(CN)_6]_2$ porous nanostructures and their CO_2 storage properties, RSC Adv. 1 (2011) 1574–1578.
[40] J. Chen, K. Huang, S. Liu, Insoluble metal hexacyanoferrates as supercapacitor electrodes, Electrochem. Commun. 10 (2008) 1851–1855.
[41] W.-J. Huang, G.-C. Fang, C.-C. Wang, A nanometer-ZnO catalyst to enhance the ozonation of 2,4,6-trichlorophenol in water, Colloids Surf., A 260 (2005) 45–51.
[42] Q. Wan, Q. Li, Y. Chen, T.-H. Wang, X. He, J. Li, C. Lin, Fabrication and ethanol sensing characteristics of ZnO nanowire gas sensors, Appl. Phys. Lett. 84 (2004) 3654–3656.
[43] N. Sekine, C.-H. Chou, W.L. Kwan, Y. Yang, ZnO nano-ridge structure and its application in inverted polymer solar cell, Org. Electron. 10 (2009) 1473–1477.
[44] A. Becheri, M. Dürr, P.L. Lo Nostro, P. Baglioni, Synthesis and characterization of zinc oxide nanoparticles: Application to textiles as UV-absorbers, J. Nanopart. Res. 10 (2008) 679–689.
[45] X. Wang, W. Cai, Y. Lin, G. Wang, C. Liang, Mass production of micro/nanostructured porous ZnO plates and their strong structurally enhanced and selective adsorption performance for environmental remediation, J. Mater. Chem. 20 (2010) 8582–8590.
[46] J.H. Lee, B.S. Kim, J.C. Lee, S. Park (Eds.), Removal of Cu^{++} ions from aqueous Cu-EDTA solution using ZnO nanopowder, Mater. Sci. Forum 486–487 (2005) 510–513.
[47] K.Y. Kumar, H. Muralidhara, Y.A. Nayaka, J. Balasubramanyam, H. Hanumanthappa, Hierarchically assembled mesoporous ZnO nanorods for the removal of lead and cadmium by using differential pulse anodic stripping voltammetric method, Powder Technol. 239 (2013) 208–216.
[48] M. Shahinpoor, K.J. Kim, Ionic polymer–metal composites: IV. Industrial and medical applications, Smart Mater. Struct. 14 (2005) 197.
[49] J. Bouclé, P. Ravirajan, J. Nelson, Hybrid polymer–metal oxide thin films for photovoltaic applications, J. Mater. Chem. 17 (2007) 3141–3153.
[50] G.A. Mahmoud, S.F. Mohamed, Removal of lead ions from aqueous solution using (sodium alginate/itaconic acid) hydrogel prepared by gamma radiation, Aust. J. Basic Appl. Sci. 6 (2012) 262–273.
[51] H. Javadian, Application of kinetic, isotherm and thermodynamic models for the adsorption of Co(II) ions on polyaniline/polypyrrole copolymer nanofibers from aqueous solution, J. Ind. Eng. Chem. 20 (2014) 4233–4241.
[52] K.Y. Foo, B.H. Hameed, Insights into the modeling of adsorption isotherm systems, Chem. Eng. J. 156 (2010) 2–10.
[53] M. Torab-Mostaedi, Biosorption of lanthanum and cerium from aqueous solutions using tangerine (*Citrus reticulata*) peel: Equilibrium, kinetic, and thermodynamic studies, Chem. Ind. Chem. Eng. Q. 19 (2013) 79–88.
[54] B.K. Sharma, N. Khare, S. Dhawan, H. Gupta, Dielectric properties of nano ZnO-polyaniline composite in the microwave frequency range, J. Alloy. Compd. 477 (2009) 370–373.
[55] H. Li, Q. Gao, L. Chen, W. Hao, Photocurrent determination ascorbic acid using an n-silicon electrode modified by platinum and cobalt hexacyanoferrate films, Sens. Actuators, B 173 (2012) 540–546.

[56] V.V. Zuev, A.V. Podshivalov, S. Bronnikov, M.A. Shishov, The oxidative polymerization of aniline as topochemical process. The statistical analysis of grain growth, Eur. Polymer J. 49 (2013) 3271–3276.
[57] R. Patil, E. Matveeva, V. Parkhutik, Simple chemical polymerization method for deposition of conducting polyaniline on surface of acrylonitrile butadiene styrene, J. Appl. Polym. Sci. 85 (2002) 1904–1910.
[58] E.C. Gomes, M.A.S. Oliveira, Chemical polymerization of aniline in hydrochloric acid (HCl) and formic acid (HCOOH) media. Differences between the Two synthesized polyanilines, Am. J. Polym. Sci. 2 (2012) 5–13.
[59] K. Ssing, D. Everett, R. Haul, L. Moscou, R. Pierotti, J. Rouquerol, T. Siemieniewsks, Reporting physisorption data for gas/solid system, Pure Appl. Chem. 57 (1985) 603–619.
[60] S. Ramaswamy, H.J. Huang, B.V. Ramarao, Separation and Purification Technologies in Biorefineries, Wiley, West Sussex, 2013.
[61] H. Masuda, K. Higashitani, H. Yoshida, Powder Technology Handbook, third ed., Taylor & Francis, Boca Raton, FL, 2006.
[62] F. Suarez-Garcia, E. Vilaplana-Ortego, M. Kunowsky, M. Kimura, A. Oya, A. Linares-Solano, Activation of polymer blend carbon nanofibres by alkaline hydroxides and their hydrogen storage performances, Int. J. Hydrogen Energy 34 (2009) 9141–9150.
[63] P. Waranusantigul, P. Pokethitiyook, M. Kruatrachue, E. Upatham, Kinetics of basic dye (methylene blue) biosorption by giant duckweed (*Spirodela polyrrhiza*), Environ. Pollut. 125 (2003) 385–392.
[64] A.R. Keshtkar, M. Irani, M.A. Moosavian, Comparative study on PVA/silica membrane functionalized with mercapto and amine groups for adsorption of Cu (II) from aqueous solutions, J. Taiwan Inst. Chem. Eng. 44 (2013) 279–286.
[65] J.P. Ros, W. Slooff, Integrated Criteria Document Cadmium, Integrated Criteria Document Cadmium, NIPHEP, 1988.
[66] A.Z. Badruddoza, Z.B. Shawon, W.J. Tay, K. Hidajat, M.S. Uddin, Fe_3O_4/cyclodextrin polymer nanocomposites for selective heavy metals removal from industrial wastewater, Carbohydr. Polym. 91 (2013) 322–332.
[67] K. Selvaraj, S. Manonmani, S. Pattabhi, Removal of hexavalent chromium using distillery sludge, Bioresour. Technol. 89 (2003) 207–211.
[68] N.R. Bishnoi, M. Bajaj, N. Sharma, A. Gupta, Adsorption of Cr(VI) on activated rice husk carbon and activated alumina, Bioresour. Technol. 91 (2004) 305–307.
[69] P.G. González, Y.B. Pliego-Cuervo, Adsorption of Cd(II), Hg(II) and Zn(II) from aqueous solution using mesoporous activated carbon produced from *Bambusa vulgaris* striata, Chem. Eng. Res. Des. 92 (2014) 2715–2724.
[70] H. Qiu, L. Lv, B.-c. Pan, Q.-j. Zhang, W.-m. Zhang, Q.-x. Zhang, Critical review in adsorption kinetic models, J. Zhejiang Univ. Sci. A 10 (2009) 716–724.
[71] H. Yuh-Shan, Citation review of Lagergren kinetic rate equation on adsorption reactions, Scientometrics, 59 (2004) 171–177.
[72] Y.-S. Ho, G. McKay, Pseudo-second order model for sorption processes, Process Biochem. 34 (1999) 451–465.
[73] M.I.El-Khaiary, Least-squares regression of adsorption equilibrium data: Comparing the options, J. Hazard. Mater. 158 (2008) 73–87.
[74] G. Limousin, J.-P. Gaudet, L. Charlet, S. Szenknect, V. Barthès, M. Krimissa, Sorption isotherms: A review on physical bases, modeling and measurement, Appl. Geochem. 22 (2007) 249–275.
[75] K. Vijayaraghavan, T. Padmesh, K. Palanivelu, M. Velan, Biosorption of nickel(II) ions onto Sargassum wightii: Application of two-parameter and three-parameter isotherm models, J. Hazard. Mater. 133 (2006) 304–308.
[76] T.W. Webi, R.K. Chakravort, Pore and solid diffusion models for fixed-bed adsorbers, AIChE J. 20 (1974) 228–238.
[77] H.Freundlich, Over the adsorption in solution, J. Phys. Chem, 57 (1906) 1100–1107.
[78] M. Roosta, M. Ghaedi, A. Daneshfar, R. Sahraei, Experimental design based response surface methodology optimization of ultrasonic assisted adsorption of safaranin O by tin sulfide nanoparticle loaded on activated carbon, Spectrochim. Acta Part A Mol. Biomol. Spectrosc. 122 (2014) 223–231.
[79] A. Dada, A. Olalekan, A. Olatunya, O. Dada, Langmuir, Freundlich, Temkin and Dubinin–Radushkevich isotherms studies of equilibrium sorption of Zn^{2+} unto phosphoric acid modified rice husk, J. Appl. Chem. 3 (2012) 38–45.
[80] H.J. Park, S.W. Jeong, J.K. Yang, B.G. Kim, S.M. Lee, Removal of heavy metals using waste eggshell, J. Environ. Sci. 19 (2007) 1436–1441.
[81] M. Torab-Mostaedi, H. Ghassabzadeh, M. Ghannadi-Maragheh, S. Ahmadi, H. Taheri, Removal of cadmium and nickel from aqueous solution using expanded perlite, Braz. J. Chem. Eng. 27 (2010) 299–308.
[82] S.F. Montanher, E.A. Oliveira, M.C. Rollemberg, Removal of metal ions from aqueous solutions by sorption onto rice bran, J. Hazard. Mater. [Evaluation Studies] 117 (2005) 207–211.
[83] D. Božić, M. Gorgievski, V. Stanković, N. Štrbac, S. Šerbula, N. Petrović, Adsorption of heavy metal ions by beech sawdust—Kinetics, mechanism and equilibrium of the process, Ecol Eng. 58 (2013) 202–206.
[84] B. Salih, A. Denizli, C. Kavaklı, R. Say, E. Pişkin, Adsorption of heavy metal ions onto dithizone-anchored poly (EGDMA-HEMA) microbeads, Talanta 46 (1998) 1205–1213.
[85] F. Ge, M.M. Li, H. Ye, B.X. Zhao, Effective removal of heavy metal ions Cd^{2+}, Zn^{2+}, Pb^{2+}, Cu^{2+} from aqueous solution by polymer-modified magnetic nanoparticles, J. Hazard. Mater. 211–212 (2012) 366–372.
[86] H. Ghassabzadeh, M. Torab-Mostaedi, A. Mohaddespour, M.G. Maragheh, S.J. Ahmadi, P. Zaheri, Characterizations of Co(II) and Pb(II) removal process from aqueous solutions using expanded perlite, Desalination 261 (2010) 73–79.
[87] N.N. Nassar, Rapid removal and recovery of Pb(II) from wastewater by magnetic nanoadsorbents, J. Hazard. Mater. 184 (2010) 538–546.
[88] L.M. Cozmuta, A.M. Cozmuta, A. Peter, C. Nicula, E.B. Nsimba, H. Tutu, The influence of pH on the adsorption of lead by Na-clinoptilolite: Kinetic and equilibrium studies, Water SA 38 (2012) 269–278.
[89] E.K. Silva, R.V.d.B. Fernandes, S.V. Borges, D.A. Botrel, F. Queiroz, Water adsorption in rosemary essential oil microparticles: Kinetics, thermodynamics and storage conditions, J. Food Eng. 140 (2014) 39–45.